
Unsupervised Neural Hidden Markov Models with a Continuous latent state space

Firas JARBOUI
 ANEO
 Centre Borelli - ENS Paris-saclay
 firasjarbou@gmail.com

Vianey PERCHET
 Criteo AI Lab
 Crest, ENSAE
 vianney.perchet@normalesup.org

Abstract

We introduce a new procedure to neuralize unsupervised Hidden Markov Models in the continuous case. This provides higher flexibility to solve problems with underlying latent variables. This approach is evaluated on both synthetic and real data. On top of generating likely model parameters with comparable performances to off-the-shelf neural architecture (LSTMs, GRUs,...), the obtained results are easily interpretable.

1 Introduction

Probabilistic Graphical Models (PGM) are standard techniques to discover highly interpretable hidden structure in data [15, 5]. Even with sequential data, off-the-shelf PGMs such as Hidden Markov Models (HMMs) are able to uncover latent patterns, as assessed by recent breakthroughs in Natural Language Processing [14, 20], Speech Recognition [21, 24] and Reinforcement Learning [3, 10, 7].

Using flexible parametric probability distributions to model the dynamics of PGMS yields better and more accurate results [12]. Given that deep neural networks are universal approximators that can eventually learn highly expressive non-convex functions [6], PGMs were recently and successfully interfaced with Artificial Neural Networks (ANNs) [8, 11]. This motivates to further bridge neural networks with HMMs, as already attempted back in the 90s [1]. Indeed, hybrid HMM/ANN models with better accuracy have been created by extracting features using neural networks : typical examples include word embeddings for unsupervised word alignment [22], convolutional neural networks for speech recognition [17], etc.

A generic approach [23] to parameter estimation in finite latent space neural HMMs, suggests to model the parameters with neural networks. In that case, gradients are back-propagated with respect to the neural network parameters during the maximisation step (M) of the Baum-Welch algorithm (the Viterbi algorithm is used in the E-step). Our main objective is to introduce a new procedure for the continuous latent state space case with a similar flavor.

More precisely, we will consider HMMs with continuous latent spaces as they encompass a very large class of non-parametric models well adapted to sequential processes. However, they were recently outperformed by recurrent neural networks (RNNs), which led to some decreasing interest [18]. On the other hand, they are highly interpretable, a key property not necessarily shared with RNN. Our main contribution is to advocate that using neural networks to estimate the parameters of the transition and emission probabilities of an HMM improves its performance up to be comparable to RNNs, while retaining the interpretability of the latent variables, therefore reaching the best of both worlds: **performances** and **interpretability**.

In details, we will investigate the theoretical framework of SMC methods to construct an optimisation algorithm that maximises the log-likelihood of the observations with respect to the model neural

network parameters. Driven by the successes of stochastic gradient descent, we also provide a stochastic and more efficient variant that preserves its experimental effectiveness.

Our methods are evaluated both on simulated and real data. The toy example is the simulation of an HMM and, without exploiting prior knowledge of the environment, our algorithm solves the parameters estimation problem. The two real-life applications use data from tourism and music. Their analysis showcase the simplicity of the implementation of our methods and, more importantly, strongly highlight the interpretability of the obtained results.

2 Neural Hidden Markov Model

In order to define ANN-based HMM, we consider two neural networks f_θ and g_θ . To alleviate notations, we use θ to denote the parameters of both ANN, even though the two networks do not necessarily share parameters. Without loss of generality, we consider a latent space $\mathcal{X} = \mathbb{R}^{d_h}$ and an observation space $\mathcal{Y} = \mathbb{R}^{d_o}$. Otherwise, an additional embedding layer would do the trick. The neural-equivalent version of HMM models (c.f. appendix A for a review of HMM models) writes as:

$$x_0 \sim \mu(x); \quad y_t \sim p_{g_\theta(x_t)}(y); \quad x_{t+1} \sim q_{f_\theta(x_t)}(x) \quad (1)$$

In practical applications, the objectives are to optimise the model parameters for multiple independent trajectories $(y_{0:T}^j)_{j=0}^K$. Thus, the log-likelihood of the observations under a given θ can be written as:

$$\mathcal{L}(\theta, (y_{0:T}^j)_{j=0}^K) = \sum_j \mathcal{L}_j(\theta, y_{0:T}^j); \quad \mathcal{L}_j(\theta, y_{0:T}^j) = \log P(y_{0:T}^j | \theta) \quad (2)$$

Equation (1) introduces non-linearity in the system, hence SMC approaches are well suited to optimise \mathcal{L} . Inspired by EM algorithms (see Appendix A.2), the particle filter from Algorithm 1 can be used to construct an asymptotically unbiased estimator of the \mathcal{Q} function.

Unfortunately, the maximiser of the following function $\hat{\mathcal{Q}}$, that approximates \mathcal{Q} , does not have an explicit form in the case of the neural HMM (in Equation (1)), because the emission and transition probabilities are no longer within the exponential family. This function $\hat{\mathcal{Q}}$ is defined by

$$\hat{\mathcal{Q}}(\theta, \theta_k) = \sum_{i,j,t} W_T^{i,j} [\log(p_{g_\theta(\hat{X}_t^{i,j})}(y_t^j)) + \log(q_{f_\theta(\hat{X}_{t-1}^{i,j})}(\hat{X}_t^{i,j}))], \quad (3)$$

where $\hat{X}_t^{i,j}$ is the i^{th} particle generated at time t for the j^{th} trajectory using an SMC method and y_t^j is the associated observation. However, it is possible, using Equation (12), to prove that a candidate parameter θ_{k+1} must satisfy:

$$\hat{\mathcal{Q}}(\theta_{k+1}, \theta_k) \geq \hat{\mathcal{Q}}(\theta_k, \theta_k) \quad (4)$$

As long as the probability distribution functions associated with the emission and transition probabilities are differentiable, the gradient of $\hat{\mathcal{Q}}$ is well defined. Moreover, functions of the form of Equation (3) are well suited for stochastic gradient-based (SGD) optimisation. In fact, the loss function l introduced in Equation (5) for a given sample $s = (y_t^j, \hat{X}_t^{i,j}, \hat{X}_{t-1}^{i,j})$ can be used to construct a new parameter θ_{k+1} , improving the likelihood:

$$l_{\theta_k}(s)(\theta) = W_T^{i,j} [\log(p_{g_\theta(\hat{X}_t^{i,j})}(y_t^j)) + \log(q_{f_\theta(\hat{X}_{t-1}^{i,j})}(\hat{X}_t^{i,j}))] \quad (5)$$

Optimising the log-likelihood with EM requires the evaluation of the posterior distribution approximation through the estimation of $[(X_{0:T}^{i,j}, (W_T^{i,j})_{i,j=0}^{N,K})]$ in the E-step, and maximising the $\hat{\mathcal{Q}}$ function in the M-step. Equation (6) provides an iterative algorithm that solves neural HMMs:

$$\begin{cases} (\hat{X}_t^{i,j})_{i,j,t}, (W_T^{i,j})_{i,j} = \text{SMC}(\theta_k, (Y_t^j)_{j,t}) \\ \theta_{k+1} = \text{SGD}(l, \theta_k, (\hat{X}_t^{i,j})_{i,j,t}, (W_T^{i,j})_{i,j}, (Y_t^j)_{j,t}) \end{cases} \quad (6)$$

2.1 Reducing computational complexity

A drawback of the EM algorithm is that the (E) step is computationally expensive. The main reason is that Equation (6) requires to run the particle filter over the full data set. When the available trajectories share a lot of similarities, we suggest that this is not necessary. An alternative is to randomly sample a batch of trajectories on which we run the optimisation. This obviously leads to faster convergence. The downside is that the same performance might not be reached; however, this is highly mitigated with a few steps at the end of training where we use the full data set in order to fine tune the parameters. We will discuss this further in the following section.

3 Experiments

We now provide experimental results to assess the relevancy and efficiency of our approach. In the synthetic example (where data are generated by some HMM), the environment is a set of target positions in a d -dimensional space, and the observations are the trajectories of a particle bouncing around them (a description of the data generating process is provided in Appendix C.1). We compare the performance of our parameter inference scheme with classical approaches to train HMMs as well as off the shelf neural network architectures (simple RNNs, LSTMs, GRUs,...). This establishes the ability of neural HMMs to provide comparable results to RNNs. In the real life examples, we use tourists GPS tracks in an open air museum, and guitar chords recordings. Experimental results of those experiments are provided in the Appendix. Based on those empirical results, we can establish that neural networks does not affect the ability of HMMs to infer interpretable latent states !

Depth of the Neural Network We compare the performance of different HMM models on the task of predicting the next observation. In the continuous HMM, the probability distributions used for the emission and transition model are Gaussian. The functions f_θ and g_θ are n -layer deep neural network used to estimate the mean and variance of the distribution, with n designating the depth of the neural network. The case where $n = 0$ is associated to vanilla HMMs where the parameters are learned using Equation (16). For the other depth values, we use Equation (6). In discrete HMMs, the transition probability distribution is a multinomial over $\{1, 2, 3, 4, 5\}$. f_θ is an n -layer neural network predicting the multinomial probabilities. In the case where $n = 0$, we use Baum-Welch to learn the parameters, otherwise we use the neural version provided in [23].

In Figure 1a, we observe that using ANN to learn the HMM parameters yields an improved performance. The obtained results from the continuous HMM case are comparable to the ones obtained from the discrete case. Deeper neural networks provided higher log-likelihoods and perform better on the one step prediction task.

Latent space dimension: Let us now compare neural HMM performance (where the parameters of the emission and transition probabilities are predicted with a 3-layer ANNs) to off-the-shelf neural network architecture used for sequence prediction (where a RNN’s output is fed to a 3-layer deep ANN). We compare performances for different latent space dimensions. In the HMM case, this corresponds to d_h , and in the other cases, it corresponds to the output dimension of the recurrent layer. In Figure 1b, we observe that at higher latent space dimension, all the models have comparable performances. However, at lower dimension, the neural HMM outperforms by a wide margin all the other off-the-shelf methods. This experiment is re-conducted with higher feature dimensions d . The obtained results, presented in Table 1, confirm this statement. These results indicate that there is a trade-off between the interpretability of the latent variables and the accuracy of the prediction to be taken into account when choosing an appropriate model. Even though recurrent neural architecture have wildly replaced HMMs in the recent years, we believe neural HMM should mitigate this trend.

Table 1: Prediction error for various feature and latent space dimensions.

FEATURE DIM (d)	MODELS	$d_h = 2$	$d_h = 3$	$d_h = 4$	$d_h = 5$	$d_h = 10$	$d_h = 20$
3	NEURAL HMM	.65±.17	.64±.17	.66±.16	.63±.16	.65±.19	.66±.18
	HMM	.92±.20	.82±.16	.82±.18	.76±.13	.71±.15	.71±.13
	RNN	.86±.06	.83±.06	.82±.07	.73±.10	.64±.09	.56±.10
	LSTM	.71±.10	.71±.08	.75±.09	.60±.09	.56±.10	.54±.10
	GRU	.82±.06	.82±.08	.73±.08	.67±.08	.56±.08	.54±.09
5	NEURAL HMM	.76±.13	.77±.12	.80±.13	.75±.14	.78±.13	.78±.13
	HMM	.98±.13	.93±.11	.87±.11	.87±.10	.81±.12	.81±.10
	RNN	.98±.01	.94±.02	.86±.06	.83±.07	.71±.07	.65±.07
	LSTM	.84±.07	.79±.07	.76±.08	.76±.07	.61±.07	.61±.07
	GRU	.87±.04	.86±.04	.80±.05	.75±.05	.66±.06	.59±.07

Number of particles: The performance of the algorithm provided in Equation (6) depends on the accuracy of the Q function approximation. The performance of the used particle filter increases as the number of particles increases as stated in Equation (14). A better approximation allows Equation (6)

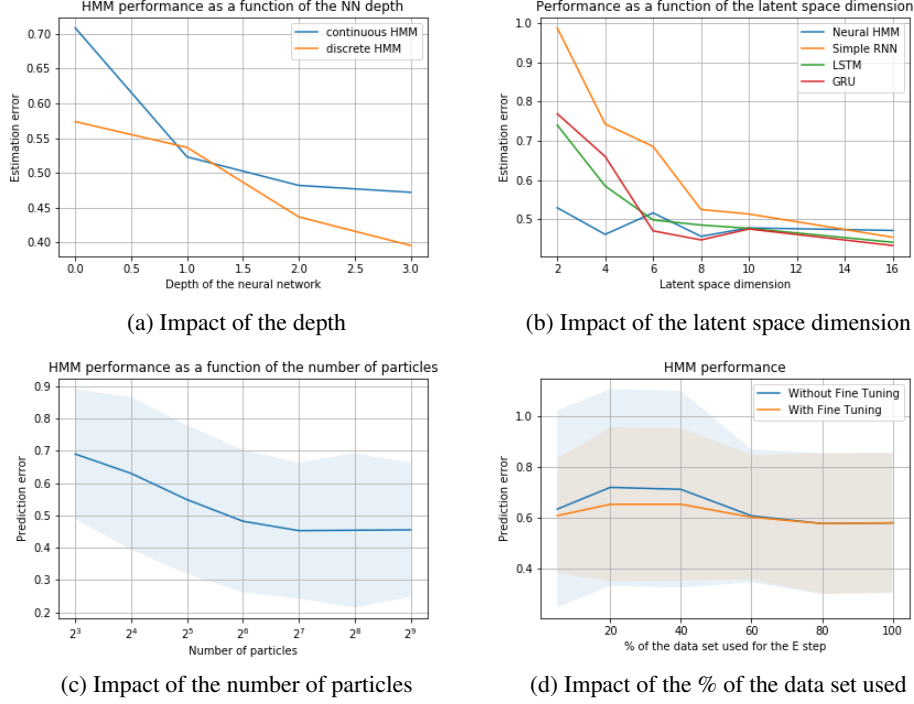


Figure 1: Performance analysis of neural HMM as a function of different parameters

to converge to better parameters at the cost of a longer training time. This improvement is however bounded. Increasing the number of particles increases linearly the computational load whereas it improves logarithmically the performance. In Figure 1c, we observe how increasing the number of particles from 8 to 128 improves the performances significantly, whereas increasing the number from 128 to 512 have a marginal impact on the prediction error. The same happens to the average log-likelihood. These experiments were conducted with a neural HMM with 3-layers ANN parameter estimators and with a 5-dimension latent space.

Reducing computational complexity: In order to evaluate the impact of applying iteratively Equation (6) on randomly sampled subsets instead of the full data set, we use the same setting with higher feature dimension ($d = 3$). we compare the prediction error reached after 100 iteration for different proportions of the data set sampled randomly in the E step. We also evaluate the same error after fine tuning the parameter with 5 iterations using the whole data set. The conclusion we draw from Figure 1d is that randomly sampling trajectories before applying Equation (6) does not affect a lot the average performance of the obtained parameters. However, the variance of the error is affected. The fine tuning steps can mitigate this issue and result in an improved performance. This procedure is especially useful in settings where an extremely large amount of data is available, such as the guitar chords example that we consider in the last section.

4 Conclusion

Neural Hidden Markov Models improve the performance of classical HMMs up to standard RNNs' while providing the same level of latent variable interpretability; thus achieving the best of both worlds. Our main contributions consist in generalising the classical approaches of HMMs training to the neural case and in providing alternatives when the data set is too large. On top of this, implementing neural HMM is a relatively easy task given the available deep learning frameworks.

The same approach presented in this paper can be adapted to more complex probabilistic graphical models. This is a big step toward reducing gaps between PGMs and RNNs, as it renders HMMs an off-the-shelf tool for practitioner and mitigates the tendency to overlook PGMs in real life applications where explainability is key.

References

- [1] Y. Bengio, R. De Mori, G. Flammia, and R. Kompe. Global optimization of a neural network-hidden markov model hybrid. In *IJCNN-91-Seattle International Joint Conference on Neural Networks*, volume 2, pages 789–794. IEEE, 1991.
- [2] A. P. Dempster, N. M. Laird, and D. B. Rubin. Maximum likelihood from incomplete data via the em algorithm. *Journal of the Royal Statistical Society: Series B (Methodological)*, 39(1):1–22, 1977.
- [3] W. Ding, S. Li, H. Qian, and Y. Chen. Hierarchical reinforcement learning framework towards multi-agent navigation. In *2018 IEEE International Conference on Robotics and Biomimetics (ROBIO)*, pages 237–242. IEEE, 2018.
- [4] R. Egger and C. Maurer. *Iscontour 2017: Tourism Research Perspectives*. BoD–Books on Demand, 2017.
- [5] D. Gunning. Explainable artificial intelligence (xai). *Defense Advanced Research Projects Agency (DARPA), nd Web*, 2, 2017.
- [6] K. Hornik, M. Stinchcombe, and H. White. Multilayer feedforward networks are universal approximators. *Neural networks*, 2(5):359–366, 1989.
- [7] F. Jarboui, C. Gruson-Daniel, A. Durmus, V. Rocchisani, S.-H. G. Ebongue, A. Depoux, W. Kirschenmann, and V. Perchet. Markov decision process for mooc users behavioral inference. In *European MOOCs Stakeholders Summit*, pages 70–80. Springer, 2019.
- [8] M. J. Johnson, D. K. Duvenaud, A. Wiltchko, R. P. Adams, and S. R. Datta. Composing graphical models with neural networks for structured representations and fast inference. In *Advances in neural information processing systems*, pages 2946–2954, 2016.
- [9] N. Kantas, A. Doucet, S. S. Singh, J. Maciejowski, and N. Chopin. On particle methods for parameter estimation in state-space models. *Statistical science*, 30(3):328–351, 2015.
- [10] S. Katt, F. A. Oliehoek, and C. Amato. Bayesian reinforcement learning in factored pomdps. In *Proceedings of the 18th International Conference on Autonomous Agents and MultiAgent Systems*, pages 7–15. International Foundation for Autonomous Agents and Multiagent Systems, 2019.
- [11] D. P. Kingma and M. Welling. Auto-encoding variational bayes. *arXiv preprint arXiv:1312.6114*, 2013.
- [12] P. Larrañaga, H. Karshenas, C. Bielza, and R. Santana. A review on probabilistic graphical models in evolutionary computation. *Journal of Heuristics*, 18(5):795–819, 2012.
- [13] R. Laubenfels. Feynman–kac formulae: Genealogical and interacting particle systems with applications, 2005.
- [14] H. Murveit and R. Moore. Integrating natural language constraints into hmm-based speech recognition. In *International Conference on Acoustics, Speech, and Signal Processing*, pages 573–576. IEEE, 1990.
- [15] A. T. Nguyen, A. Kharosekar, M. Lease, and B. Wallace. An interpretable joint graphical model for fact-checking from crowds. In *Thirty-Second AAAI Conference on Artificial Intelligence*, 2018.
- [16] J. Osmalsky, J.-J. Embrechts, M. Van Droogenbroeck, and S. Pierard. Neural networks for musical chords recognition. In *Journées d’informatique Musicale*, pages 39–46, 2012.
- [17] D. Palaz, M. Magimai-Doss, and R. Collobert. End-to-end acoustic modeling using convolutional neural networks for hmm-based automatic speech recognition. *Speech Communication*, 108:15–32, 2019.
- [18] M. Panzner and P. Cimiano. Comparing hidden markov models and long short term memory neural networks for learning action representations. In *International Workshop on Machine Learning, Optimization, and Big Data*, pages 94–105. Springer, 2016.
- [19] M. K. Pitt and N. Shephard. Filtering via simulation: Auxiliary particle filters. *Journal of the American statistical association*, 94(446):590–599, 1999.
- [20] N. Ranjan, K. Mundada, K. Phaltane, and S. Ahmad. A survey on techniques in nlp. *International Journal of Computer Applications*, 134(8):6–9, 2016.

- [21] S. Renals, N. Morgan, H. Bourlard, M. Cohen, and H. Franco. Connectionist probability estimators in hmm speech recognition. -, 1994.
- [22] T. Songyot and D. Chiang. Improving word alignment using word similarity. In *Proceedings of the 2014 Conference on Empirical Methods in Natural Language Processing (EMNLP)*, pages 1840–1845, 2014.
- [23] K. Tran, Y. Bisk, A. Vaswani, D. Marcu, and K. Knight. Unsupervised neural hidden markov models. *arXiv preprint arXiv:1609.09007*, 2016.
- [24] S. Xue, H. Jiang, L. Dai, and Q. Liu. Speaker adaptation of hybrid nn/hmm model for speech recognition based on singular value decomposition. *Journal of Signal Processing Systems*, 82(2):175–185, 2016.

A Mathematical Background

A.1 Hidden Markov Models with Continuous latent state space

Let us describe formally HMMs. They are defined by some latent state space \mathcal{X} and observation space \mathcal{Y} . Two sequences of observations $(y_t)_{t=0}^T \in \mathcal{Y}$ and latent states $(x_t)_{t=0}^T \in \mathcal{X}$, where $T \in \mathbb{N}$, are generated as follows. The first state x_0 is chosen at random according to some underlying distribution μ . Then the first observation y_0 is drawn accordingly to $p_\theta(\cdot|x_0)$, a probability distribution over \mathcal{Y} . This distribution is called the *emission probability distribution*. The dynamics of x_t is then controlled by the *transition probability distribution* $q_\theta(\cdot|x_{t-1})$ as in a standard Markov chain. Formally, variables satisfy the following equation:

$$x_0 \sim \mu(x); \quad y_t \sim p_\theta(y|x_t); \quad x_{t+1} \sim q_\theta(x|x_t) \quad (7)$$

The estimation of the model hidden parameters is usually done by the optimisation of the log-likelihood of the observations with respect to the model parameters, i.e.:

$$\theta^* = \operatorname{argmax}_\theta \mathcal{L}(\theta, (y_t)_{t=0}^T) = \operatorname{argmax}_\theta \log (P(y_{0:T}|\theta)). \quad (8)$$

As usual, the first step to compute \mathcal{L} is to marginalise this quantity with respect to the latent variables:

$$P(y_{0:T}|\theta) = \int P(y_{0:T}, x_{0:T}|\theta) dx_{0:T}, \quad (9)$$

where the joint distribution can be rewritten into:

$$P(y_{0:T}, x_{0:T}|\theta) = \mu(x_0) \times \prod_{t=0}^T [p_\theta(y_t|x_t) \times q_\theta(x_{t+1}|x_t)]. \quad (10)$$

A popular choice to maximise the log likelihood \mathcal{L} is the class of EM algorithms. Given the initialisation θ_0 , a sequence of estimated parameters is constructed as follows:

$$\theta_{k+1} = \operatorname{argmax}_\theta \mathcal{Q}(\theta, \theta_k); \quad \mathcal{Q}(\theta, \theta_k) = \int P(x_{0:T}|y_{0:T}, \theta_k) \log P(y_{0:T}, x_{0:T}|\theta) dx_{0:T} \quad (11)$$

The key property of EM techniques is that the sequence $(\mathcal{L}(\theta_k, (y_t)_{t=0}^T))_k$ is non decreasing. In fact a stronger result [2] even states that:

$$(\mathcal{L}(\theta, (y_t)_{t=0}^T))_k \geq (\mathcal{L}(\theta_k, (y_t)_{t=0}^T))_k \iff \mathcal{Q}(\theta, \theta_k) \geq \mathcal{Q}(\theta_k, \theta_k) \quad (12)$$

Moreover, the EM algorithm, is favored to gradient based methods for its numerical stability [2].

A.2 Particle Filters for HMMs

In order to optimise the log-likelihood with respect to θ , see Equation (11), the posterior distribution of the latent states $P(x_{0:T}|y_{0:T}, \theta)$ must be evaluated. We propose to do this with particle filters, a class of SMC methods. The principle is to generate N latent state candidates, re-sample them according to their likelihood in the model, and use them to generate N candidate latent states for the next time step. By sampling likely trajectories, and weighing them according to their corresponding likelihood, a good approximation of the posterior is constructed. Various implementation of the particle filters can be considered [19].

Algorithm 1 The bootstrap filter

```

1: Procedure:  $SMC(\theta, (Y_t)_{t=0}^T)$ 
2:  $X_0^i \sim \mu_\theta \forall i \in [0, N]$ 
3:  $W_0^i \propto P(Y_0|X_0^i, \theta) \times \mu_\theta(X_0^i)$  s.t.  $\sum_i W_0^i = 1$ 
4:  $\hat{X}_0^i \sim \sum_i W_0^i \delta_{X_0^i}$ 
5: for  $t \in [1, T]$  do
6:    $X_t^i \sim P(x|\hat{X}_{t-1}^i, \theta) \forall i \in [0, N]$ 
7:    $W_t^i \propto P(Y_t|X_t^i, \theta) \times W_{t-1}^i$  s.t.  $\sum_i W_t^i = 1$ 
8:    $\hat{X}_{0:t}^i \sim \sum_i W_t^i \delta_{X_{0:t}^i}$ 
9: end for
10: Return:  $(\hat{X}_{0:T}^i)_{i=0}^N, (W_T^i)_{i=0}^N$ 

```

The pseudo-code of the bootstrap variation of these filters is presented in Algorithm 1. We have denoted by $(X_{0:T}^i)_{i=0}^N$ the latent trajectories created by the particle filters, and by $(W_T^i)_{i=0}^N$, their weights; those two quantities are the keystones of the posterior distribution. Indeed, an asymptotically unbiased estimator is defined by [13, 9]:

$$\hat{P}(x_{0:T}|y_{0:T}, \theta) = \sum_i W_T^i \delta_{\hat{X}_{0:T}^i}(dx_{0:T}). \quad (13)$$

A key property of the particles based estimation of the posterior function is that it can also be used to construct asymptotically unbiased estimates of smooth additive functionals of the following form [13]:

$$\mathcal{S}_T^\theta = \int \log \left[\prod_{t=0}^T s_t(x_{t-1:t}) \right] P(x_{0:T}|y_{0:T}, \theta) dx_{0:T}$$

Substituting the posterior distribution with its estimate gives an approximation $\hat{\mathcal{S}}_T^\theta$ satisfying [13]:

$$|\mathbb{E}[\hat{\mathcal{S}}_T^\theta] - \mathcal{S}_T^\theta| \leq F_\theta \frac{T}{N}, \quad F_\theta \in \mathbb{R}^*, \quad (14)$$

where the expectation is with respect to the particle filter. Equation (10) implies that the \mathcal{Q} function defined in Equation (11) has the same form as \mathcal{S}_T^θ . Notice that this corresponds to the special case where $s_0 = \mu(x_0)$ and $s_{t+1}(x_{t:t+1}) = p_\theta(y_t|x_t) \times q_\theta(x_{t+1}|x_t)$. As a consequence, an asymptotically unbiased estimator of the \mathcal{Q} function is:

$$\hat{\mathcal{Q}}(\theta, \theta_k) = \sum_i W_T^i \log P(y_{0:T}, \hat{X}_{0:T}^i|\theta). \quad (15)$$

This optimises the log-likelihood \mathcal{L} using an approximation of the EM algorithm presented in Equation (11) by computing at the k^{th} iteration $\text{argmax}_\theta \hat{\mathcal{Q}}(\theta, \theta_k)$.

A.3 Implementation

In practice, when $p_\theta(y|x_t)$ and $q_\theta(x|x_t)$ are chosen from the exponential family, solving an HMM with the EM algorithm boils down to computing a summary statistic of the $\mathcal{Q}(\theta, \theta_k)$ function using a particle filter. The maximising argument of $\hat{\mathcal{Q}}(\theta, \theta_k)$ can be explicitly computed through a suitable function $\Lambda((Y_t)_{t=0}^T, (\hat{X}_{0:T}^i)_{i=0}^N, (W_T^i)_{i=0}^N)$. The standard open source HMM solvers (such as pomegranate and HMMlearn) propose the following algorithm:

$$\begin{cases} (\hat{X}_{0:T}^i)_{i=0}^N, (W_T^i)_{i=0}^N = SMC(\theta_k, (Y_t)_{t=0}^T) \\ \theta_{k+1} = \Lambda((Y_t)_{t=0}^T, (\hat{X}_{0:T}^i)_{i=0}^N, (W_T^i)_{i=0}^N) \end{cases} \quad (16)$$

B Higher order Neural HMMs

HMMs can also easily incorporate bounded memory processes. Indeed, let $\tau_e, \tau_t \geq 0$ be two memory window sizes, then Equation (7) can be transformed into:

$$x_0 \sim \mu(x); \quad y_t \sim p_{g_\theta}(x_t, y_{t-\tau_e:t-1})(y); \quad x_{t+1} \sim q_{f_\theta}(x_t, y_{t-\tau_t:t})(x) \quad (17)$$

This model can be seen as a neural HMM of order (τ_e, τ_t) . All the previous theoretical results hold true, in particular Equation (6) can be used to optimise the parameters of this model by rewriting the loss function from Equation (5) as:

$$l_{\theta_k}(s)(\theta) = W_T^{i,j} [\log (p_{g_\theta}(\hat{X}_t^{i,j}, y_{t-\tau_e:t-1}^j)(y_t^j)) + \log (q_{f_\theta}(\hat{X}_{t-1}^{i,j}, y_{t-\tau_t:t}^j)(\hat{X}_t^{i,j}))] \quad (18)$$

This enables HMMs to piggy-ride on all the progress that Deep Learning is currently undergoing.

C Complementary experimental results

C.1 Synthetic setting: data generating process

We consider a set of targets $(X_i)_1^N$. Particles move toward their current targets X_{i_t} : the direction of the movement is sampled according to a Gaussian $\mathcal{N}(X_{i_t}, \sigma)$. Once a particle is ϵ close to X_{i_t} , its new target is sampled according to a uniform distribution, as modelled by Equation (19).

$$\begin{cases} i_t &= \begin{cases} \sim \mathcal{U}_{[1,2,\dots,N]} & \text{if } \|y_t - X_{i_{t-1}}\| \leq \epsilon \\ i_{t-1} & \text{if } \|y_t - X_{i_{t-1}}\| > \epsilon \end{cases} \\ x_t &\sim \mathcal{N}(X_{i_t}, \sigma) \\ y_{t+1} &= y_t + \frac{x_t - y_t}{\|x_t - y_t\|} \end{cases} \quad (19)$$

Figure 2 illustrates an example of the generated trajectories (y_t) and latent states (x_t), where the number of components is $N = 5$ and the feature dimension is $d = 2$.

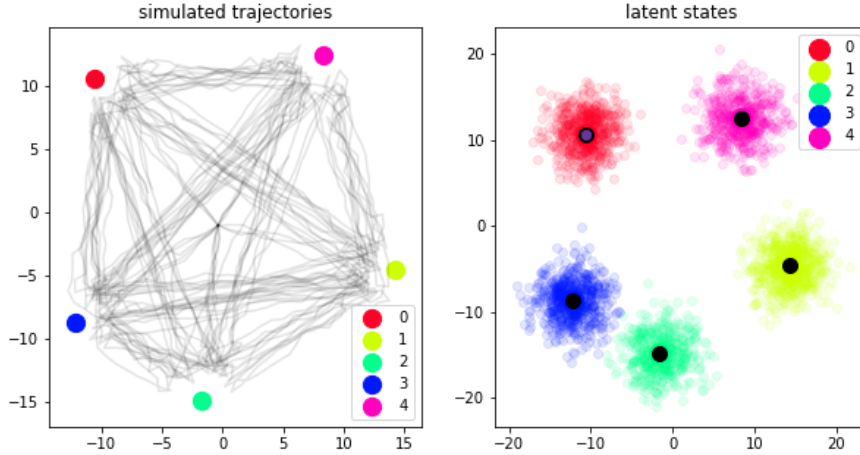


Figure 2: Synthetic data set

C.2 Real-life data sets

The real strength of using HMMs is the interpretability of the latent states. We explore two real-life data sets in order to provide qualitative proof that this aspect is not lost when using neural HMMs.

C.2.1 Open air museum

We consider the data set gathered during a study conducted in an open air museum in Austria [4]. 200 visitors of the *Freilicht museum* were equipped with GPS-Trackers and their behaviours were qualitatively analysed [4]. Given that a visitor's intention and preferences can explain his path when visiting the museum, the HMM model lend itself to explain the observed trajectories. We use the data from the same study and model the trajectories using Equation (1) where y_t is the position of the tourist at time t . We use Gaussian distribution for the emission and transition, where the parameters are estimated using 3-layer ANNs. The latent variables are encoded in 2 dimensions. Maximising

the Log-likelihood of the model using Equation (6) converges in a few iterations. The parameters are then used to compute the latent states of a given trajectory. Clustering these latent states using K-mean, reveals two visiting behaviours of the museum as illustrated in Figure 3. When reviewing the website of the museum, we discover that the visitors have the choice between discovering the attractions by walking or using a railway ride. The train trajectory can be matched to the blue data point and the walking itinerary to the orange ones. Extracting these patterns in an unsupervised way using only the position of the visitors and despite the fact that the walking and the railway paths intersect, is a good example of how highly interpretable neural HMMs can be.

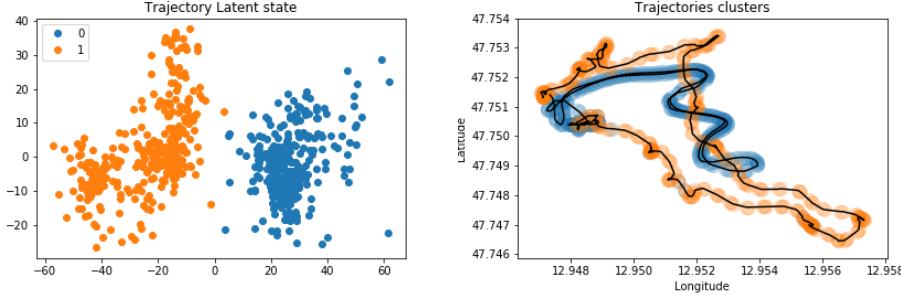


Figure 3: GPS track clusters

C.2.2 Guitar chords

Our objective is to provide a prototype music recognition system that relies on neural HMMs, in an unsupervised manner. Let us describe more precisely this example.

Setting: We limit the analysis to 10 basic guitar chords (A, Am, Bm, C, D, Dm, E, Em, F, G) for complexity reason, as standard music related research [16]. The objective is to train a classifier that decomposes a melody into a sequence of these chords.

Successful attempts are based on the so-called Pitch Class Profile (PCP) [16]. Roughly speaking, the PCP is a set of features obtained through a spectral analysis, followed by a Fourier transform, of the signal, i.e., the melody. Mathematically, it is a mapping from $[0, T]$ to \mathbb{R}^{12} . Very roughly speaking, it associates to each instant $t \in [0, T]$ of the melody different energy levels of the 12 keys of a piano octave.

Dataset : A dataset of guitar chords recordings (200 per chord) in various settings (an anechoic chamber / a noisy environment), using four different guitars, and with different playing techniques [16] is used. These sequences can be seen as random pieces of music.

In theory, each chord’s ideal PCP would always activate the same different subsets of harmonics; However, the surrounding noise, the type of guitar, etc. are many different reasons that explain actual variations in PCP. In practice, a chord might not be recoverable directly from a single PCP observation: the associated PCP diagram, may vary depending on the player technique, the order in which the different notes of a chord are heard.

neuralHMM: The chord successions can be well modeled by higher order neural HMMs, introduced in Equation (17). The observations y_t are the PCP while the latent variables are the chords played.

We recall that a higher order neural HMM is defined by two hyper-parameters (the window memory) and two neural networks. The experimental results corresponds to

- Hyper-parameters: $\tau_e = 1$ and $\tau_t = 15$.
- Emission network g_θ : a two layer neural network (width of 32 neurons)
- Transition network f_θ : an LSTM constructs an embedding of the previous observations $y_{t-\tau_t-1:t-1}$; they are concatenated with the previous representations and fed to a two layer neural network (same width of 32 neurons).

The optimization of the different neural nets (see Equation (6)) require samples of trajectories; for illustration purpose, we fix their lengths to 5 guitar chords (see such a PCP illustrated in Figure 4

corresponding to the sequence ('C', 'E', 'D', 'E', 'F').) and we choose 5 chord recordings at random in the chord data-set. The total number of possible 'chord trajectories' is prohibitively large, up to 3.10^{16} , so we either limit its size (for Equation (6)) or we simply use the stochastic variant of the algorithm.

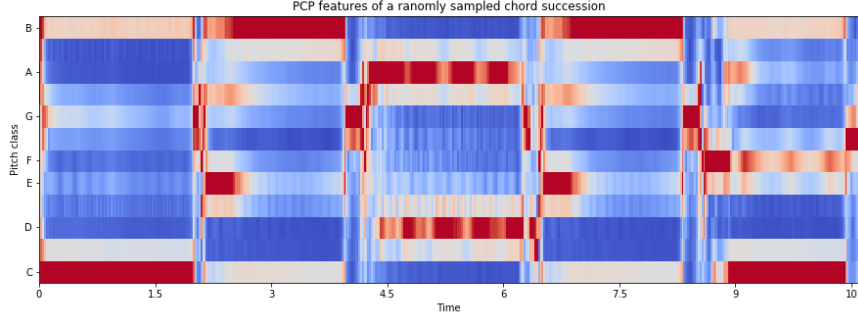
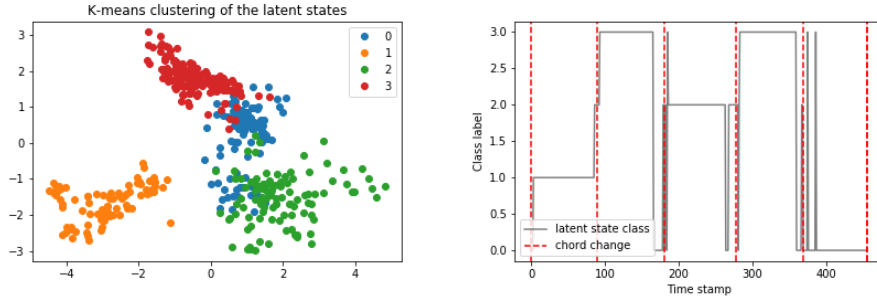


Figure 4: PCP of a randomly sampled guitar chords

Results: Performance wise, we observe in Table 2 that neural HMMs out-performs vanilla recurrent neural networks when using low latent space dimension. In the following, we will use $d_h = 5$. After the training, we extract the latent states using Algorithm 1. Going back to the example of the trajectory of Figure 4, we further cluster the associated representations into four classes (number of unique chords used in this sample) using K-means. This is illustrated in Figure 5a after a PCA of the latent states coordinate.



(a) Latent state embedding clustered using K-mean

(b) Class evaluation over time

Figure 5: Performance analysis of the regretted detection delay as a function of the cutting threshold

Table 2: Prediction error for various latent space dimensions.

MODELS	$d_h = 2$	$d_h = 5$	$d_h = 10$	$d_h = 20$
N-HMM	.30 ± .02	.28 ± .03	.31 ± .03	.33 ± .04
HMM	1.04 ± .05	.65 ± .03	.46 ± .03	.56 ± .04
RNN	.64 ± .07	.41 ± .06	.31 ± .07	.29 ± .05
LSTM	.62 ± .06	.42 ± .07	.30 ± .07	.29 ± .07
GRU	.60 ± .05	.40 ± .07	.31 ± .08	.30 ± .08

To highlight even more the powerful results of our method, we filter the audio file according to the identified clusters. Figure 5b reveals that each one of them can be associated with a particular chord. Indeed, the dashed red lines are associated with the time step where a new guitar chord is being played, the black line evaluates the cluster label of the audio file over time according to the learned latent states. Those clusters almost coincide.

Furthermore, we can even reconstruct the typical PCP of a particular chord. We represent them in Figure 6, where the PCP of the latent spaces in the same specific cluster are concatenated for illustration purposes.

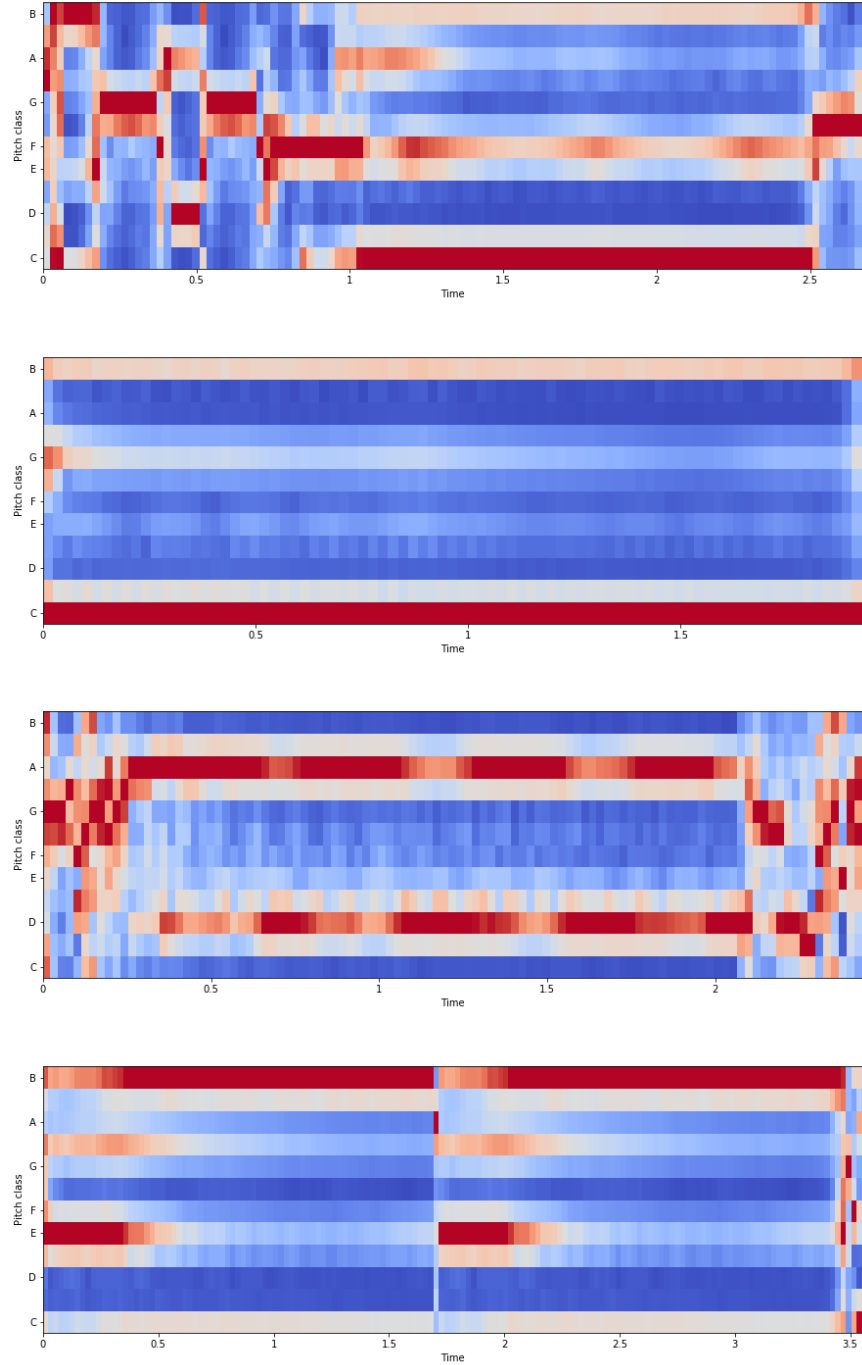


Figure 6: PCP associated to the latent states classes